Rare-earth Zirconate $Ln_2Zr_2O_7$ (Ln: La, Nd, Gd and Dy) Powders, Xerogels and Aerogels: Preparation, Structure and Properties

*Jorge Torres-Rodriguez [†, *], Vanessa Gutierrez-Cano[‡], Melita Menelaou[†, *], Jaroslav Kaštyl[†], Jaroslav Cihlář[†], Serhii Tkachenko[†], Jesús A. González[‡], József Kalmár[⊥,§], István Fábián[⊥,§], István Lázár[⊥,§], Ladislav Čelko[†], Jozef Kaiser[†]*

[†] Central European Institute of Technology, Brno University of Technology, Purkyňova 123, 612 00 Brno, Czech Republic

[‡] Department of Earth Sciences and Condensed Matter Physics, University of Cantabria, 39 005, Santander, Spain

[⊥] Department of Inorganic and Analytical Chemistry, University of Debrecen, Egyetem tér 1, Debrecen, H-4032 Hungary

§ MTA-DE Redox and Homogeneous Catalytic Reaction Mechanisms Research Group,

Egyetem tér 1, Debrecen, H-4032 Hungary

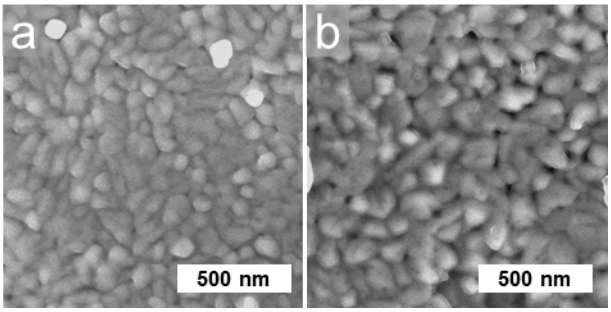

Fig. S1. Scanning electron microscopy: Surface morphology of the calcined powders at 1000 °C/5 h; a) $Nd_2Zr_2O_7$; b) $Dy_2Zr_2O_7$.

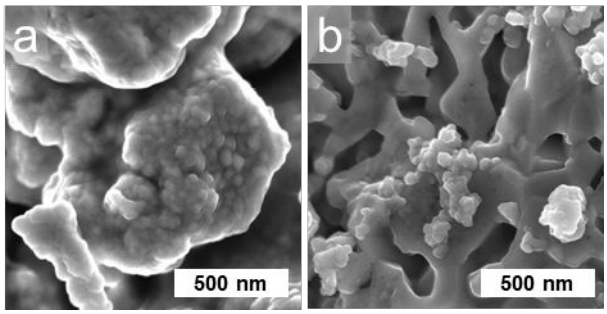

Fig. S2. Scanning electron microscopy: Surface morphology of the calcined xerogels at 1000 °C/5 h; a) $Nd_2Zr_2O_7$; b) $Dy_2Zr_2O_7$.

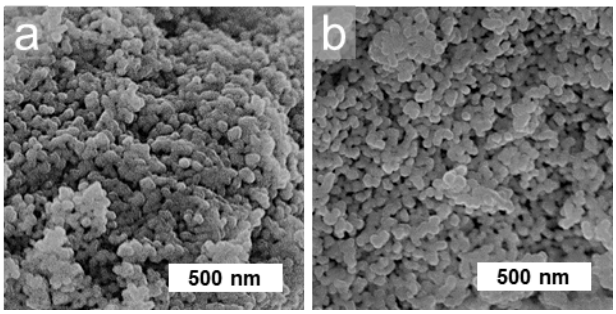

Fig. S3. Scanning electron microscopy: Surface morphology of the calcined aerogels at 1000 °C/5 h; a) $Nd_2Zr_2O_7$; b) $Dy_2Zr_2O_7$.

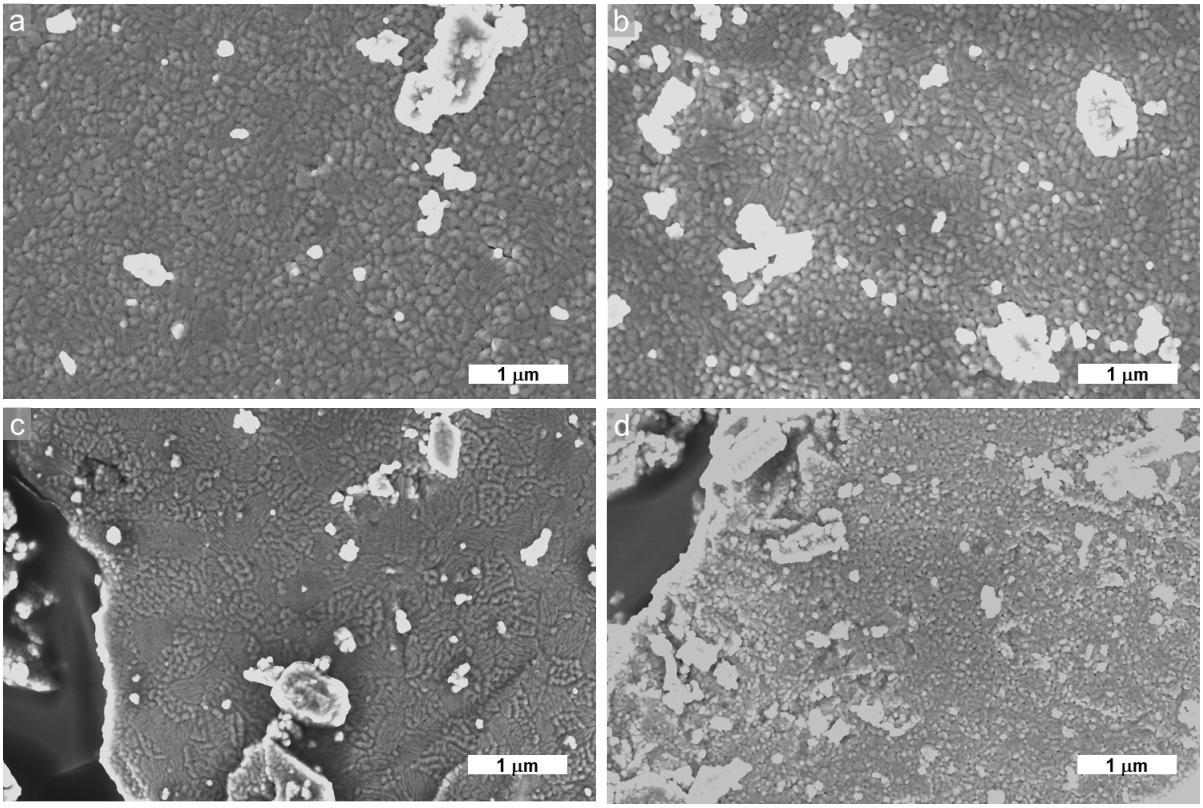

Fig. S4. Scanning electron microscopy: Lower magnification surface morphology of the calcined powders at 1000 °C/5 h; a) $La_2Zr_2O_7$; b) $Nd_2Zr_2O_7$; c) $Gd_2Zr_2O_7$; d) $Dy_2Zr_2O_7$.

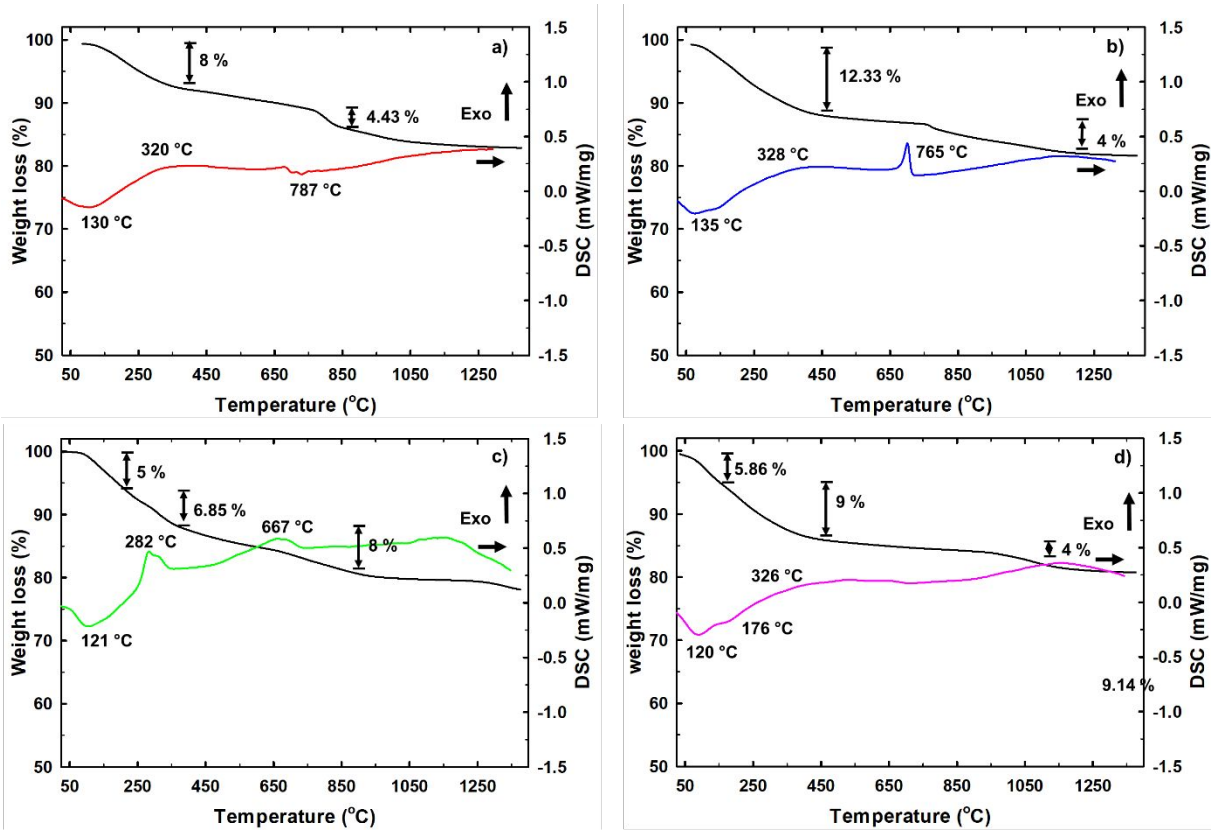

Fig. S5. DSC/TGA patterns (from 25 to 1400 °C) of the as-obtained LnZP; a) LZP; b) NZP c) GZP; d) DZP.

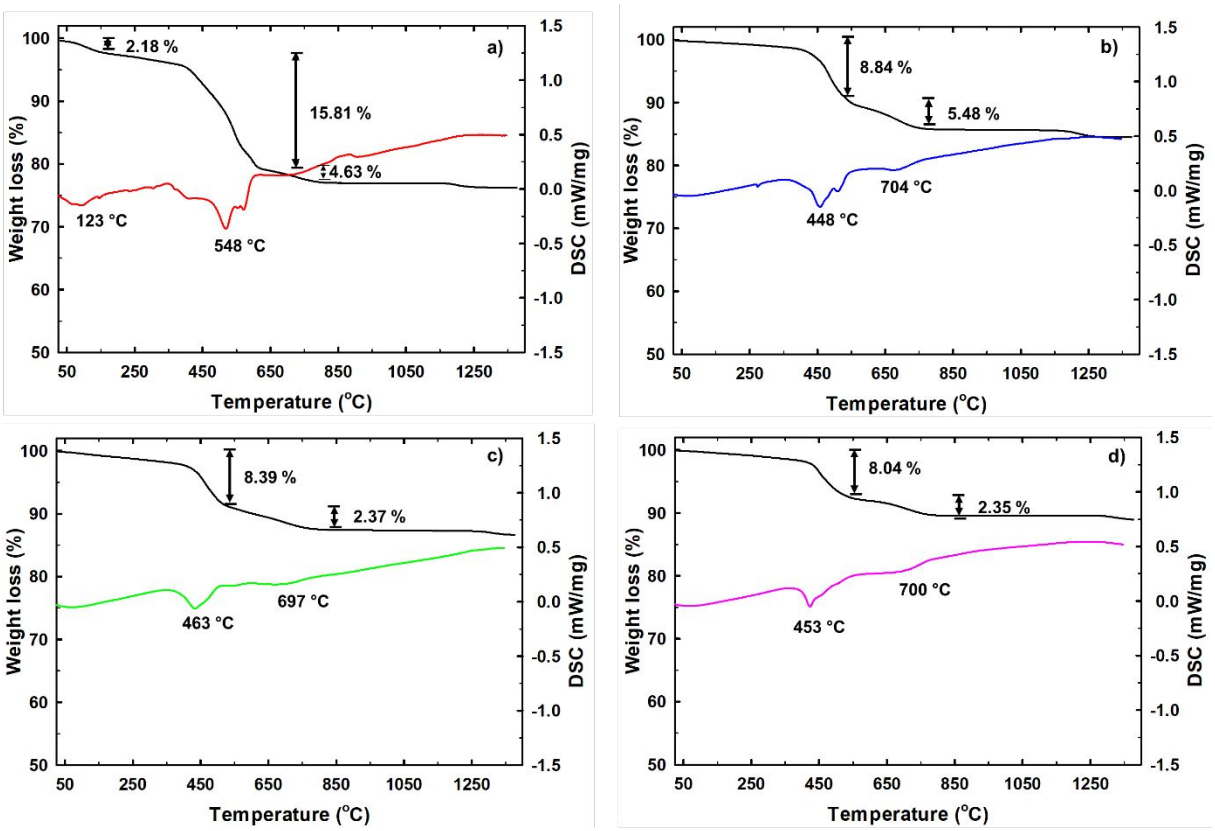

Fig. S6. DSC/TGA patterns (from 25 to 1400 °C) of the as-obtained LnZX; a) LZX; b) NZX c) GZX; d) DZX.

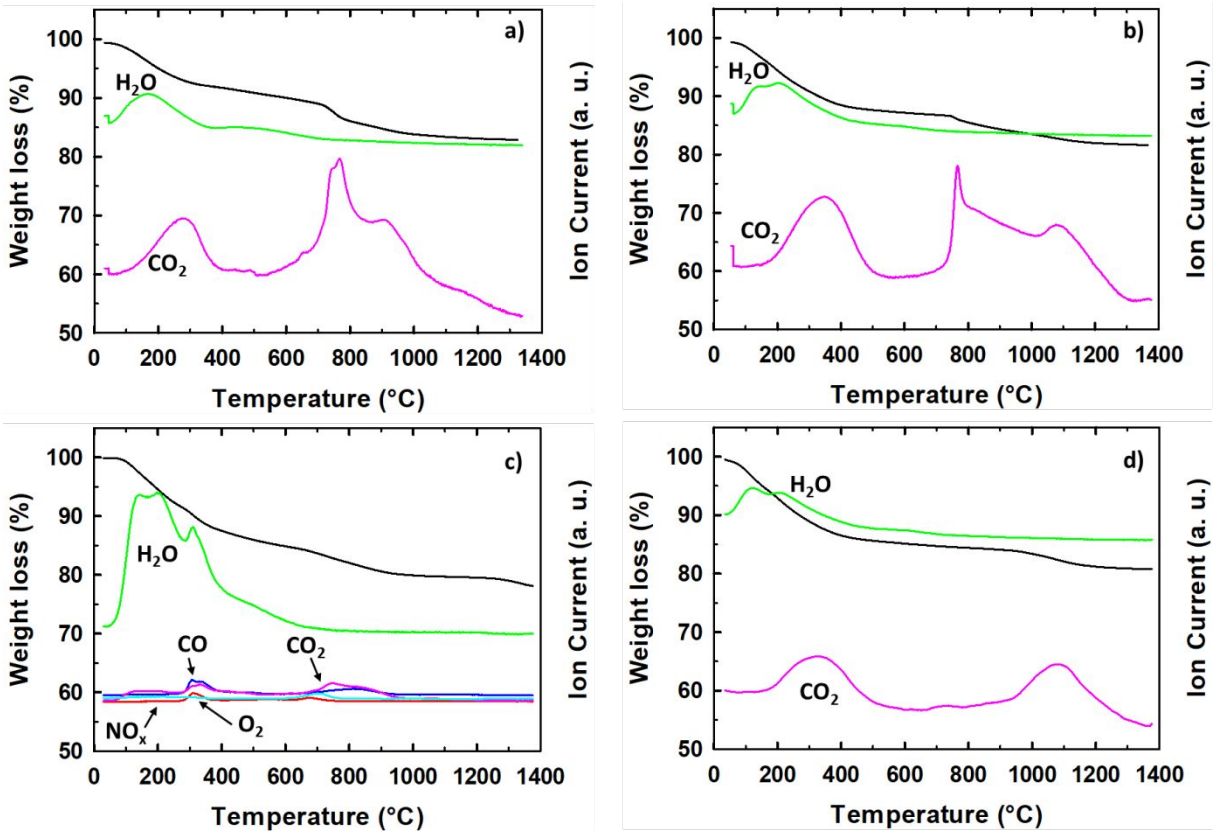

Fig. S7. Thermogravimetric analysis (TGA) and mass spectrometry (MS) of the as-prepared LnZP. Comparison of the simultaneous TG signal and MS signal at *m/z*: H_2O: 18, CO: 28, O_2: 32, CO_2: 44, and NO_x: 14; 30; 46, Graph a) LZP; b) NZP; c) GZP; d) DZP.

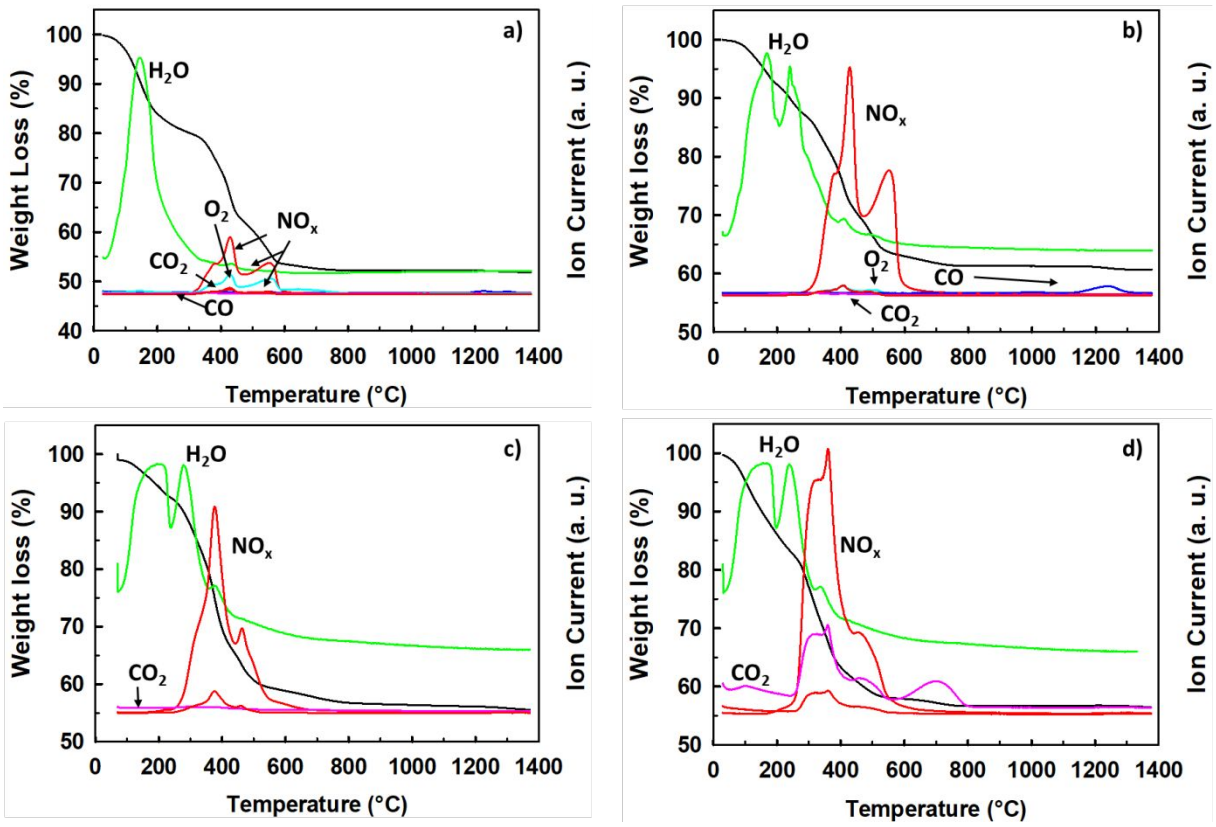

Fig. S8. Thermogravimetric analysis (TGA) and mass spectrometry (MS) of the as-prepared LnZX. Comparison of the simultaneous TG signal and MS signals at *m/z*: H_2O: 18, CO: 28, O_2: 32, CO_2: 44, and NO_x: 14; 30; 46, Graph a) LZX; b) NZX; c) GZX; d) DZX.

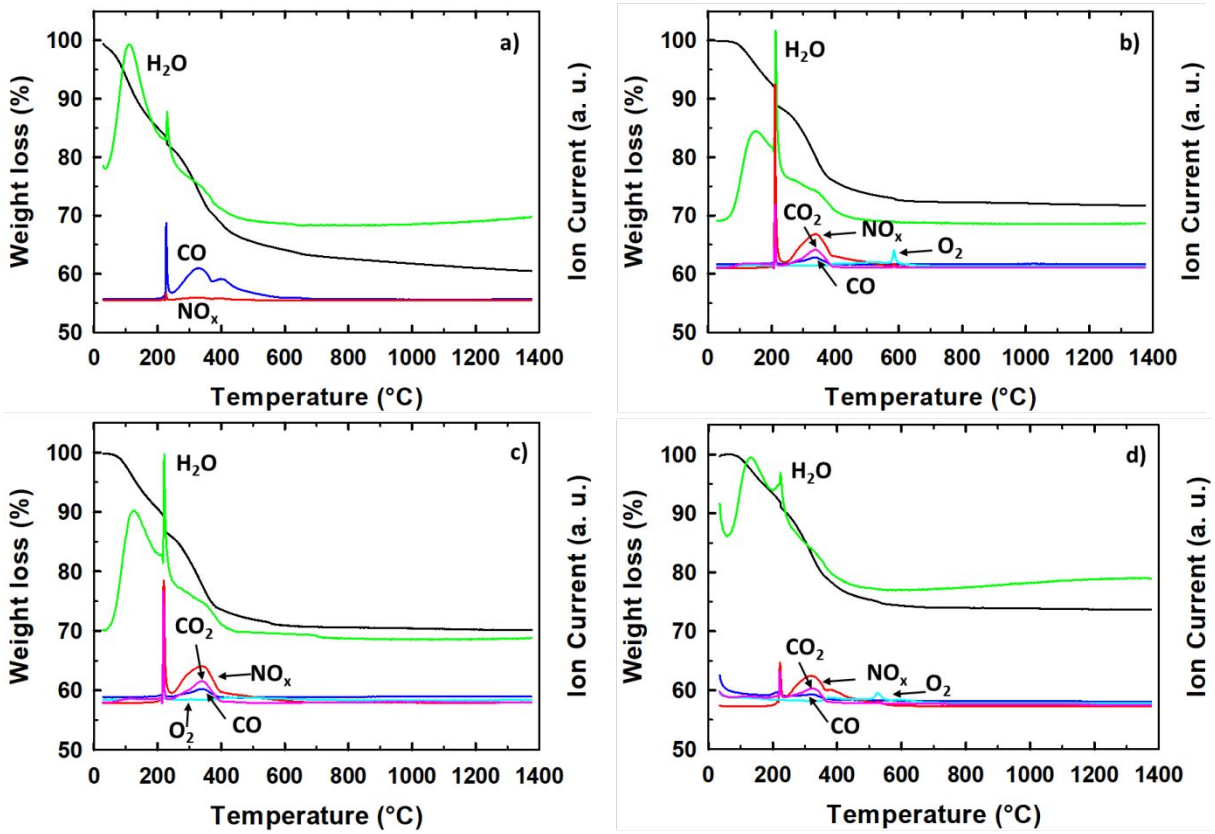

Fig. S9. Thermogravimetric analysis (TGA) and mass spectrometry (MS) of the as-prepared LnZA. Comparison of the simultaneous TG signal and MS signal at *m/z*: H_2O: 18, CO: 28, O_2: 32, CO_2: 44, and NO_x: 14; 30; 46, Graph a) LZA; b) NZA; c) GZA; d) DZA.

Fig. S10. Pictures of the as-obtained materials; a) LZP; b) LZX and c) LZA

Synthesis route	Heat treatment	Crystalline phases	Reference
Sol-gel	Drying 60-300 °C Annealing 600 °C/2h	Mainly $Bi_2Ti_2O_7$ pyrochlore with minor $Bi_4Ti_3O_{12}$, $Bi_{12}TiO_{20}$, and TiO_2	[4]
	Drying 400 °C/30 min Annealing 600 °C/1h	$Bi_2Ti_2O_7$ Pyrochlore	[5]

Table S1. Different synthesis routes to produce rare-earth zirconate powders.

	Drying 80 °C Annealing 700-900 °C1/h	$Y_2Ti_2O_7$ Pyrochlore	[6]
Hydrothermal	200 °C/24h	$Gd_2Zr_2O_7$ Fluorite	[7]
	80 °C/48h	$Ca_2Bi_2O_7$ Pyrochlore $Sr_2Bi_2O_7$ Pyrochlore	[8]
	200 °C/20h	$Gd_2Zr_2O_7$:Tb^{3+} Fluorite	[9]
Co-precipitation	Drying 80 °C/24h Annealing 300-1100/5h	$Gd_2Zr_2O_7$ Fluorite, Pyrochlore	[10]
	Drying 120 °C/12h Annealing 500 °C/10h	$Ln_2Zr_2O_7$ (Ln = Gd^{3+}, Nd^{3+}, Sm^{3+}), Fluorite, Pyrochlore	[11]
	Drying 80°C/12h Annealing 550 °C/16h	$Bi_2Ti_2O_7$ Pyrochlore	[12]
Molten salts	Drying 90 °C/1h Annealing 1000-1200 °C/1-8h	$Yb_2Ti_2O_7$ Pyrochlore	[13]
	Annealing 650 °C/6h	$La_2Zr_2O_7$ Fluorite $La_2Hf_2O_7$ Fluorite $Er_2Zr_2O_7$ Fluorite	[14]
	Annealing 650 °C/1-12h	$La_2Hf_2O_7Eu^{3+}$ Pyrochlore	[15]
Mecanochemical	Annealing 800, 1400 °C/12h	$Gd_2Zr_2O_7$ (Gd substitution by different Ln^{3+}), Fluorite, Pyrochlore	[16]
	Annealing 1500 °C/6h	$Gd_{1.6}Ln_{0.4}Zr_2O_7$ (Ln = La^{3+}, Nd^{3+}, Sm^{3+},Dy^{3+} and Er^{3+}), Fluorite, Pyrochlore	[17]
	Annealing 1500 °C/72h	$Gd_2Ce_xZr_{2-x}O_7$ ($0 \leq x \leq 2$), Pyrochlore, Fluorite	[18].

Table S2. Summary of the thermal processes at the different temperature ranges.

Material	Loss	Temperature range	Reference
LnZP	H_2O	90 – 400	[1]
	CO_2	200 – 500; 600 – 1000	[3]
	CO	270 – 380; 600 – 950	[3]
	O_2	630 – 730	[3]
	NOx	210 – 350; 630 – 750	[1, 3]
LnZX	H_2O	90 – 400	[19]
	CO_2	245 – 800	[19]
	CO	1100 – 1350	[19]
	O_2	320 – 600	[3]
	NOx	250 – 650	[1, 3]
LnZA	H_2O	100 – 400	[2]
	CO_2	200 – 230; 250 – 420	[2]
	CO	200 – 600	[2]
	O_2	550 – 610; 500 – 550	[2]
	NOx	200 – 500	[2]

REFERENCES

[1] H. Chen, Y. Gao, Y. Liu, H. Luo. Coprecipitation synthesis and thermal conductivity of $La_2Zr_2O_7$. *J. Alloy. Compd.,* 480 (**2009**), 843. DOI: 10.1016/j.jallcom.2009.02.081

[2] J. Torres-Rodriguez, J. Kalmár, M. Menelaou, L. Čelko,K. Dvořak, J. Cihlář, J. Cihlař, J. Kaiser, E. Győri, P. Veres, I. Fábián, I. Lázár. Heat treatment induced phase transformations in zirconia and yttria-stabilized zirconia monolithic aerogels. *J. Supercrit. Fluid,* 20 (**2019**), 109. DOI: 10.1016/j.supflu.2019.02.011

[3] E. D. Ion, B. Malič, I. Arčon, J. P. Gomilšek, A. Kodre, M. Kosec. Characterization of lanthanum zirconate prepared by a nitrate-modified alkoxide synthesis route: From sol to crystalline powder. *J. Eur. Ceram. Soc.,* 30 (**2010**), 569. DOI: 10.1016/j.jeurceramsoc.2009.04.009

[4] S. S. Kim, M. H. Park, J. K. Chung, W. Kim. Structural study of a sol-gel derived pyrochlore $Bi_2Ti_2O_7$ using a Rietveld analysis method based on neutron scattering studies. *J. Appl. Phys.*, 105 (**2009**), 061641. DOI: doi.org/10.1063/1.3056166

[5] H. Zhou, T. Park, S. Wong. Synthesis, characterization, and photocatalytic properties of pyrochlore $Bi_2Ti_2O_7$ nanotubes. *J. Mater. Res.*, 21 (**2006**), 2941. DOI: 10.1557/jmr.2006.0362

[6] Z. S. Chen, W. P. Gong, T. F. Chen, S. L. Li. Synthesis and characterization of pyrochlore-type yttrium titanate nanoparticles by modified sol-gel method. *Bull. Mater. Sci.*, 34 (**2011**), 429. DOI: 10.1007/s12034-011-0116-2

[7] Z. Tang, Z. Huang, J. Qi, X. Guo, W. Han, M. Zhou, S. Peng, T. Lu. Synthesis and characterization of $Gd_2Zr_2O_7$ defect-fluorite oxide nanoparticles via a homogeneous precipitation-solvothermal method. *RSC. Adv.*, 7 (**2017**), 54980. DOI: 10.1039/C7RA11019G

[8] M. Saiduzzaman, T. Takei, S. Yanagida, N. Kumada, H. Das, H. Kyokane, S. Wakazaki, M. Azuma, C. Moriyoshi, Y. Kuroiwa. Hydrothermal Synthesis of Pyrochlore-Type Pentavalent Bismuthates $Ca_2Bi_2O_7$ and $Sr_2Bi_2O_7$. *Inorg. Chem.*, 58 (**2019**), 1759. DOI: 10.1021/acs.inorgchem.8b03596 I

[9] L. Gao, H. Zhu, L. Wang, G. Ou. Hydrothermal synthesis and photoluminescence properties of $Gd_2Zr_2O_7$:Tb^{3+} phosphors. *Mater. Lett.*, 65 (**2011**), 1360. DOI: 10.1016/j.matlet.2011.02.004

[10] L. Zhou, Z. Huang, J. Qi, Z. Feng, D. Wu, W. Zhang, X. Yu, Y. Guan, X. Chen, L. Xie, K. Sun, T. Lu. Thermal-Driven Fluorite–Pyrochlore–Fluorite Phase Transitions of $Gd_2Zr_2O_7$ Ceramics Probed in Large Range of Sintering Temperature. *Metall. Mater. Trans. A.*, 47 (**2016**), 623. DOI: 10.1007/s11661-015-3234-4

[11] J. Wu, X. Wei, N. P. Padture, P. G. Klemens, M. Gell, E. García, P. Miranzo, M. I. Osendi. Low-Thermal-Conductivity Rare-Earth zirconates for potential thermal-barrier-coating applications. *J. Am. Ceram. Soc.*, 85 (**2002**). DOI: 10.1111/j.1151-2916.2002.tb00574.x

[12] V. Kumar, R. Sharma, S. Kumar, M. Kaur, J. D. Sharma. Enhancement in the photocatalytic activity of $Bi_2Ti_2O_7$ nanopowders synthesised via Pechini vs Co-Precipitation method. *Ceram. Int.*, 45 (**2019**), 20386. DOI: 10.1016/j.ceramint.2019.07.015

[13] L. Matthew, M. Hand, C. Stennett, C. Neil, C. Hyatt. Rapid low temperature synthesis of a titanate pyrochlore by molten salt mediated reaction. *J. Eur. Ceram. Soc.*, 32 (**2012**), 3211. DOI: 10.1016/j.jeurceramsoc.2012.04.046

[14] Y. Mao, X. Guo, J. Y. Huang, K. L. Wang, J. P. Chang. Luminescent Nanocrystals with $A_2B_2O_7$ Composition Synthesized by a Kinetically Modified Molten Salt Method. *J. Phys. Chem. C.*, 113 (**2009**), 1204. DOI: 10.1021/jp807111h

[15] J. P. Zuniga, S. K. Gupta, M. Abdou, Y. Mao. Effect of Molten Salt Synthesis Processing Duration on the Photo- and Radioluminescence of UV-, Visible-, and X-ray-Excitable $La_2Hf_2O_7$:Eu^{3+} Nanoparticles. *ACS Omega.*, 3 (**2018**), 7757. DOI: 10.1021/acsomega.8b00987

[16] A. F. Fuentes, S. M. Montemayor, M. Maczka, M. Lang, R. C. Ewing, U. Amador. A Critical Review of Existing Criteria for the Prediction of Pyrochlore Formation and Stability. *Inorg. Chem.,* 57 (**2018**), 12093. DOI: 10.1021/acs.inorgchem.8b01665

[17] J. A. Díaz-Guillén, O. J. Durá, M. R. Díaz-Guillén, E. Bauer, M. A. López de la Torre, A. F. Fuentes. Thermophysical properties of $Gd_2Zr_2O_7$ powders prepared by mechanical milling: Effect of homovalent Gd^{3+} substitution. *J. Alloy. Compd.*, 649 (**2015**), 1145. 10.1016/j.jallcom.2015.07.146

[18] X. Lu, Y. Ding, X. Shu, X. Mao, X. Wang. Preparation and heavy-ion irradiation effects of $Gd_2Ce_xZr_{2-x}O_7$ ceramics. *RSC Adv.*, 5 (**2015**), 64247. DOI: 10.1039/C5RA13241J

[19] S. Wang, W. Li, S. Wang, Z. Chen. Synthesis of nanostructured $La_2Zr_2O_7$ by a non-alkoxide sol–gel method: From gel to crystalline powders. *J. Eur. Ceram. Soc.*, 35 (**2015**), 105. DOI: 10.1016/j.jeurceramsoc.2014.08.032